nature structural & molecular biology

Conformational dynamics in substrate-binding domains influences transport in the ABC importer GlnPQ

Giorgos Gouridis[1–3], Gea K Schuurman-Wolters[1,3], Evelyn Ploetz[2,3], Florence Husada[2], Ruslan Vietrov[1], Marijn de Boer[1,2], Thorben Cordes[2] & Bert Poolman[1]

The conformational dynamics in ABC transporters is largely elusive. The ABC importer GlnPQ from *Lactococcus lactis* has different covalently linked substrate-binding domains (SBDs), thus making it an excellent model system to elucidate the dynamics and role of the SBDs in transport. We demonstrate by single-molecule spectroscopy that the two SBDs intrinsically transit from open to closed ligand-free conformation, and the proteins capture their amino acid ligands via an induced-fit mechanism. High-affinity ligands elicit transitions without changing the closed-state lifetime, whereas low-affinity ligands dramatically shorten it. We show that SBDs in the closed state compete for docking onto the translocator, but remarkably the effect is strongest without ligand. We find that the rate-determining steps depend on the SBD and the amino acid transported. We conclude that the lifetime of the closed conformation controls both SBD docking to the translocator and substrate release.

ATP-binding cassette (ABC) transporters are integral membrane proteins found in all kingdoms of life[1]. The importers are involved in uptake of cellular building blocks and nutrients and also in large-scale accumulation of compatible solutes for cell-volume regulation[2,3] and of signaling molecules for intercellular communication[4–6]. ABC exporters are involved in extrusion of drugs and antibiotics[7], lipid translocation[8], antigen presentation[5] and numerous other functions[9]. Both importers and exporters consist of two transmembrane domains (TMDs) and two cytoplasmic nucleotide-binding domains (NBDs), which power transport through hydrolysis of ATP. Besides TMDs and NBDs, the ABC importers use SBDs or substrate-binding proteins (SBPs) to capture substrates from the environment and deliver them to the translocator. The SBDs are fused to the TMD, whereas SBPs are separate polypeptides, either present in the periplasm or associated with the membrane via a lipid or protein anchor[10]. A subset of ABC transporters has two or even three SBDs fused in tandem[10,11], thus giving rise to four or six receptor domains per functional complex. Despite the difference in the number of SBDs and their linkage to the cell surface, the basic transport mechanism of ABC importers could be similar. However, very little is known of how ABC importers interact with multiple (and structurally distinct) SBDs. Do the SBDs operate independently of each other, and do they function via a similar mechanism? Do multiple SBDs increase the substrate spectrum and/or transport capacity? Do the SBDs compete for docking onto the TMD, and in which conformation do they interact[12–17]? Importantly, the transporters with multiple SBDs fused to the TMDs offer unique possibilities for probing the rate-determining steps in translocation and the influence of the dynamics of SBDs in translocation. In this study, we focus on GlnPQ (**Fig. 1a**) from the Gram-positive bacterium *L. lactis*, which uses two different SBDs for import of asparagine, glutamine and glutamate[11,18].

The overall fold of the two SBDs of GlnPQ is very similar even though their primary sequences diverge by more than 50%. Numerous crystal structures of SBDs[19] and some structural information from NMR are available[20,21], but the mechanism of ligand binding ('induced fit' versus 'conformational selection') is still under debate[22,23]. What remains elusive, however, is how the binding mechanism influences the transport process. Moreover, there is no consensus on the conformations of SBDs that lead to a productive translocation cycle. In one model[15,16] for maltose transport in *Escherichia coli*, the closed ligand-bound SBD binds to the inward-facing conformation of the TMD and triggers a pretranslocation state. The transition to the outward-facing conformation upon binding of ATP facilitates the opening of the SBD to release the substrate into the TMD cavity. Subsequent hydrolysis of ATP (and release of inorganic phosphate (P_i) and ADP) resets the system to the inward-facing conformation and completes the transport cycle. In a contradicting model[17], the open state of the SBD interacts with the TMD in the outward-facing conformation, and this then allows the binding of maltose. Upon subsequent hydrolysis of ATP, the transporter converts to the inward-facing conformation and releases the maltose into the cytoplasm.

To discriminate between the different models of substrate delivery and translocation by ABC importers and to understand the role of the individual SBDs in the transport process, a variety of different studies have been carried out. To date, a number of crystal structures are available of full-length ABC importers with a single soluble SBP[15,24–26]. Crystal structures provide crucial snapshots of discrete states of the translocation cycle but do not resolve the dynamics of the processes.

[1]Department of Biochemistry, Groningen Biomolecular Sciences and Biotechnology Institute, University of Groningen, Groningen, the Netherlands. [2]Molecular Microscopy Research Group, Zernike Institute for Advanced Materials, University of Groningen, Groningen, the Netherlands. [3]These authors contributed equally to this work. Correspondence should be addressed to T.C. (t.m.cordes@rug.nl) or B.P. (b.poolman@rug.nl).

Received 15 August; accepted 6 November; published online 8 December 2014; doi:10.1038/nsmb.2929

Additionally, 'bulk' biochemical experiments cannot provide insights into rare and/or transient events that are crucial for the transport process because these are lost in the ensemble averaging. Here, we used single-molecule Förster resonance energy transfer (smFRET) to probe conformational dynamics of the SBDs and correlated these findings with isothermal titration calorimetry (ITC) to determine the specificity and thermodynamics of ligand binding. In addition, we monitored the overall transport process to relate differences in binding activity and protein conformation to translocation efficiency. With this unique combination of techniques, we present new mechanistic insight into the transport mechanism of ABC importers: (i) SBDs of GlnPQ bind their ligands via an induced-fit mechanism; (ii) the lifetime of the closed ligand-bound state determines the rate of transport; and (iii) the closed ligand-free state of SBD2 inhibits transport via SBD1.

RESULTS

GlnPQ is essential for amino acid uptake

We recently determined the structures and amino acid specificity of SBD1 and SBD2 of GlnPQ (**Fig. 1a**) from both pathogenic and non-pathogenic bacteria[11] (summary of relevant K_d values for ligand binding in **Supplementary Fig. 1c** and K_d values of the SBD derivatives analyzed here). Briefly, SBD1 binds asparagine with high affinity (K_d = 0.2 µM) as well as glutamine with low affinity (K_d = 92 µM), whereas SBD2 binds only glutamine with high affinity (K_d = 0.9 µM). To determine the contribution of the SBDs on amino acid transport and cell growth, we deleted the chromosomal GlnPQ-encoding genes (denoted *glnPQ*) in *L. lactis* NZ9000 and complemented the null strain (GKW9000) in *trans* with *glnPQ* variants. *In vivo* uptake experiments showed that transport of glutamine no longer occurred in *L. lactis* GKW9000 (**Fig. 1b**) either complemented or not complemented with GlnPQ-ΔSBD, whereas some residual asparagine uptake activity (due to an endogenous transport system) was present (**Fig. 1c**). GlnPQ, expressed in *trans*, restored the uptake of both amino acids (**Fig. 1b–d**). The rate of transport of glutamine was faster than that of asparagine, a result that is in line with the higher requirements for this essential amino acid. The mechanistic basis for this difference is presented below.

Relation between substrate binding and transport kinetics

We next assessed the relationship between substrate binding and the kinetics of the whole transport process. We examined GlnPQ and 'simplified' transporters with either of the two SBDs deleted (**Fig. 1a**; GlnPQ-SBD1 and GlnPQ-SBD2). In GlnPQ, SBD2 is proximal to the translocator, whereas SBD1 is distal (**Fig. 1a**). GlnPQ-SBD1 mediates transport of both asparagine (**Fig. 1c**) and glutamine (**Fig. 1b**). The maximal transport rate (V_{max}) of glutamine was approximately two-fold higher than that of asparagine (**Fig. 1b**,**c**). In contrast, GlnPQ-SBD2 mediates transport of only glutamine, with an approximately two-fold-higher V_{max} than that of GlnPQ-SBD1 (**Fig. 1b**,**c**). In all cases, amino acid transport followed Michaelis-Menten kinetics (**Supplementary Fig. 1b**; K_m and V_{max} values summarized in **Supplementary Fig. 1c**). The higher rates of transport of GlnPQ-SBD1 and GlnPQ-SBD2 relative to GlnPQ reflect higher expression levels (**Fig. 1d**) and more complete processing of the transporters with a single SBD. The K_m value for glutamine transport via SBD2 approaches the K_d value for its binding to SBD2. In terms of Michaelis-Menten kinetics, a $K_m/K_d \approx 1$ would be consistent with a model in which the translocation (rate constant) is slow compared to the dissociation of ligand and thus is probably rate determining. However, the K_m value for asparagine transport via SBD1 is two orders of magnitude higher than the corresponding K_d value, whereas the K_m value for glutamine transport is approximately seven-fold lower than the K_d value. These remarkable observations suggest that the rate-determining step in the overall translocation can vary with the SBD used and the substrate transported. To incorporate these findings in a unifying model, we investigated how conformational dynamics of SBDs influence transport.

Conformational states at the single-molecule level

In the induced-fit mechanism[27], the substrate triggers the formation of the closed ligand-bound (CL) conformation upon binding to the open state (O; **Fig. 2a**). In the conformational-selection model, fast dynamics to a partially closed or closed state (PC or C) occurs without the involvement of a ligand[21,23,28]. Ligand binding stabilizes the PC or C form and thereby drives the equilibrium to the CL form (**Fig. 2a**).

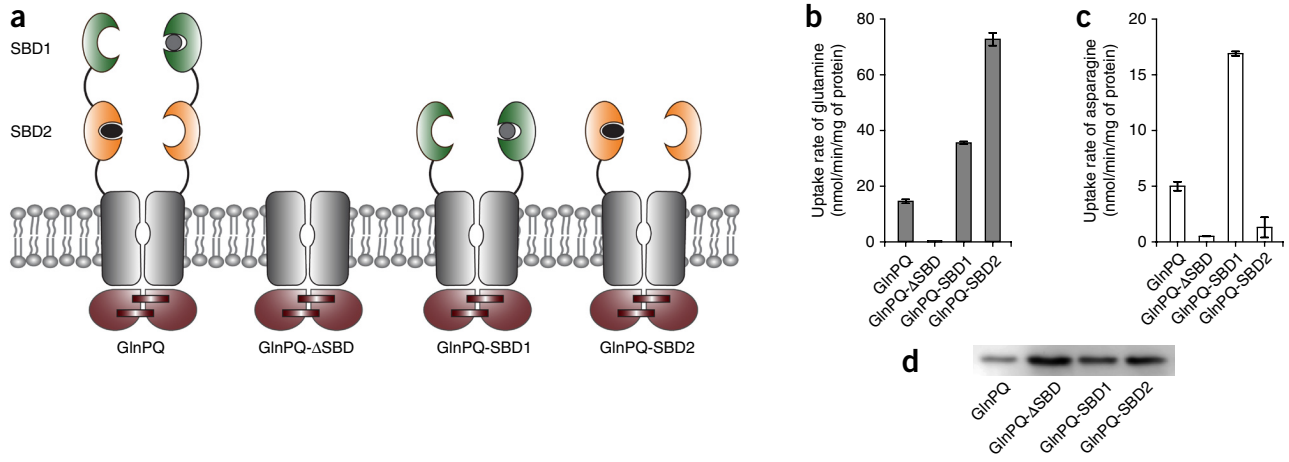

Figure 1 ABC importer GlnPQ and amino acid transport. (**a**) Schematic of GlnPQ, featuring two fused SBDs (SBD1 (green) and SBD2 (orange)) per TMD, as well as of GlnPQ derivatives lacking both SBDs (GlnPQ-ΔSBD) or carrying only a single SBD (GlnPQ-SBD1 and GlnPQ-SBD2). (**b**,**c**) Whole-cell uptake assays with 250 µM [^{14}C]glutamine (**b**) or 250 µM [^{3}H]asparagine (**c**) in *L. lactis* GKW9000 complemented *in trans* with GlnPQ or the indicated derivatives (as described in Online Methods). The uptake rate was determined as shown in **Supplementary Figure 1a**. Error bars, s.e.m. calculated from independent cell cultures (for GlnPQ, n = 12; for GlnPQ-SBD1 and GlnPQ-SBD2, n = 3: for GlnPQ-ΔSBD, n = 2 with average value and no s.e.m. presented). (**d**) Relative amounts of transporter determined by immunostaining with anti-histidine antibody (as described in Online Methods). Uncropped image of the gel blot is shown in **Supplementary Data Set 1**.

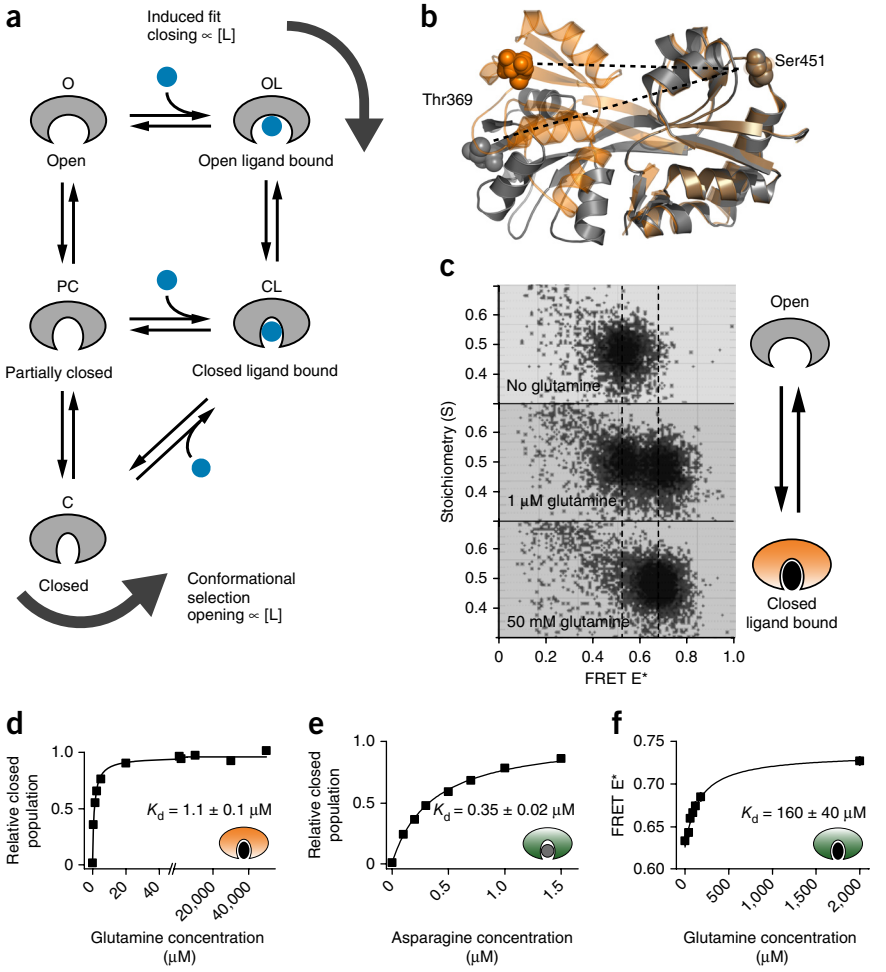

Figure 2 Ligand-binding mechanisms and protein conformational changes probed in solution by confocal ALEX spectroscopy. (**a**) Conformational transitions in SBDs according to the induced-fit or the conformational-selection binding mechanisms. ∝ [L], proportional to ligand concentration. (**b**) Crystal structure of the open ligand-free state of SBD2 (gray, PDB 4KR5 (ref. 11)), superimposed onto the structure of one of the rigid domains of the closed ligand-bound state (orange, PDB 4KQP[11]). Residues mutated to cysteine for labeling are shown in spheres. The residues are 49.0 Å apart in the open state and come to 40.1 Å in the closed state. (**c**) Confocal single-molecule analysis with ALEX of SBD2 labeled stochastically with Cy3B- and Atto 647N-maleimide. (**d**–**f**) Ligand dissociation constants (K_d) derived from ALEX E*-S histograms, as presented in **Supplementary Figure 2c**–**e**. (**d**,**e**) K_d values of SBD2(T369C S451C) for glutamine (**d**) and SBD1(T159C G87C) for asparagine (**e**), obtained from the ratio of areas (CL/(O + CL)) between open and closed ligand-bound populations at the indicated substrate concentrations. (**f**) The K_d value of SBD1(T159C G87C) for glutamine, obtained by plotting the peak value of FRET from a Gaussian fit as a function of its concentration. We obtained similar results after labeling other positions in the SBDs (**Supplementary Fig. 3**) or using other fluorophores.

We examined the conformational states of the SBDs by smFRET[29] and observed conformational changes as a change in FRET efficiency (**Fig. 2c** and **Supplementary Fig. 2b**–**e**). By design, the open conformation of the protein should feature a low FRET efficiency, whereas the closed conformation should have a higher FRET efficiency. The distances between fluorophores were designed to be between 3 and 6 nm in both states; typical distance changes are between 0.5 and 1.3 nm (**Supplementary Fig. 2a**). We determined ligand binding by stepwise addition of substrate, monitoring the hypothesized transition from O to CL. The relationship between FRET efficiency and interprobe distance, and thus the actual conformational change, requires free fluorophore rotation, which we verified by anisotropy measurements (**Supplementary Fig. 3c**).

SBD2 labeled at T369C and S451C (**Fig. 2b**) showed a single population normally distributed around an apparent FRET value (E*) of 0.52 (**Fig. 2c**). Saturating concentrations of glutamine (more than ten-fold K_d) shifted the population to a high FRET state (E* = 0.68), whereas we observed both states at concentrations around the K_d of SBD2 for glutamine (**Fig. 2c**). In agreement with expectations from crystal structures, the low FRET state corresponds to the O state, whereas the high FRET state is indicative of the CL state. The apparent K_d value (K_d^{app}) is in excellent agreement with values determined by ITC (**Fig. 2d** and **Supplementary Fig. 1c**). Concordantly with the ITC data, asparagine did not affect the E* of SBD2 (data not shown).

SBD1 labeled at T159C and G87C shifted from a low-FRET (O) conformation to the CL state upon binding of asparagine. Again, the calculated K_d^{app} was consistent with ITC data (**Fig. 2e** and **Supplementary Fig. 1c**). In contrast to the effect of asparagine, saturating concentrations of glutamine shifted SBD1 from the open state at E* = 0.63 to an intermediate value of E* = 0.74, which is lower than that observed with asparagine (E* = 0.83). Given the time resolution of alternating-laser excitation (ALEX) experiments[30,31] and the width of the FRET distributions, this is likely to be caused by fast conformational dynamics between an O and a PC or C state on the submillisecond time scale. In the presence of glutamine, the SBD1 population gradually shifted to higher FRET values, and the peak had its maximal width at concentrations close to the K_d value (**Supplementary Fig. 2e**). The peak shift as a function of glutamine concentration (**Fig. 2f**) yielded a K_d^{app} of 160 ± 40 µM, which is in reasonable agreement with the ITC value of 92 ± 16 µM (**Supplementary Fig. 1c** and **Supplementary Table 1**).

We conclude from the smFRET measurements in solution that (i) apo-SBD1 and apo-SBD2 are predominantly (>95%) in the open conformation; (ii) SBD1 and SDB2 transit to a closed state upon binding of high-affinity ligands, presumably via an induced-fit mechanism; and (iii) binding of glutamine to SBD1 is of low affinity and induces fast transitions between two distinct conformational states.

SBD1 and SBD2 exhibit intrinsic dynamics between O and C

To investigate the dynamics of conformational changes in SBDs, we carried out smFRET experiments with surface-bound proteins, using a confocal scanning microscope (**Fig. 3a**)[32]. In accordance with the ALEX experiments, both SBDs were predominantly in the open conformation when no ligand was present (SBD2 in **Fig. 3b**; SBD1 in **Fig. 3c**); representative fluorescent time traces of the apoproteins (**Fig. 3b**,**c**) showed E* values of ~0.50 for SBD2 and ~0.63 for SBD1, which we assign to the open ligand-free state of the proteins. Importantly, in the absence of substrate, we observed rare transitions

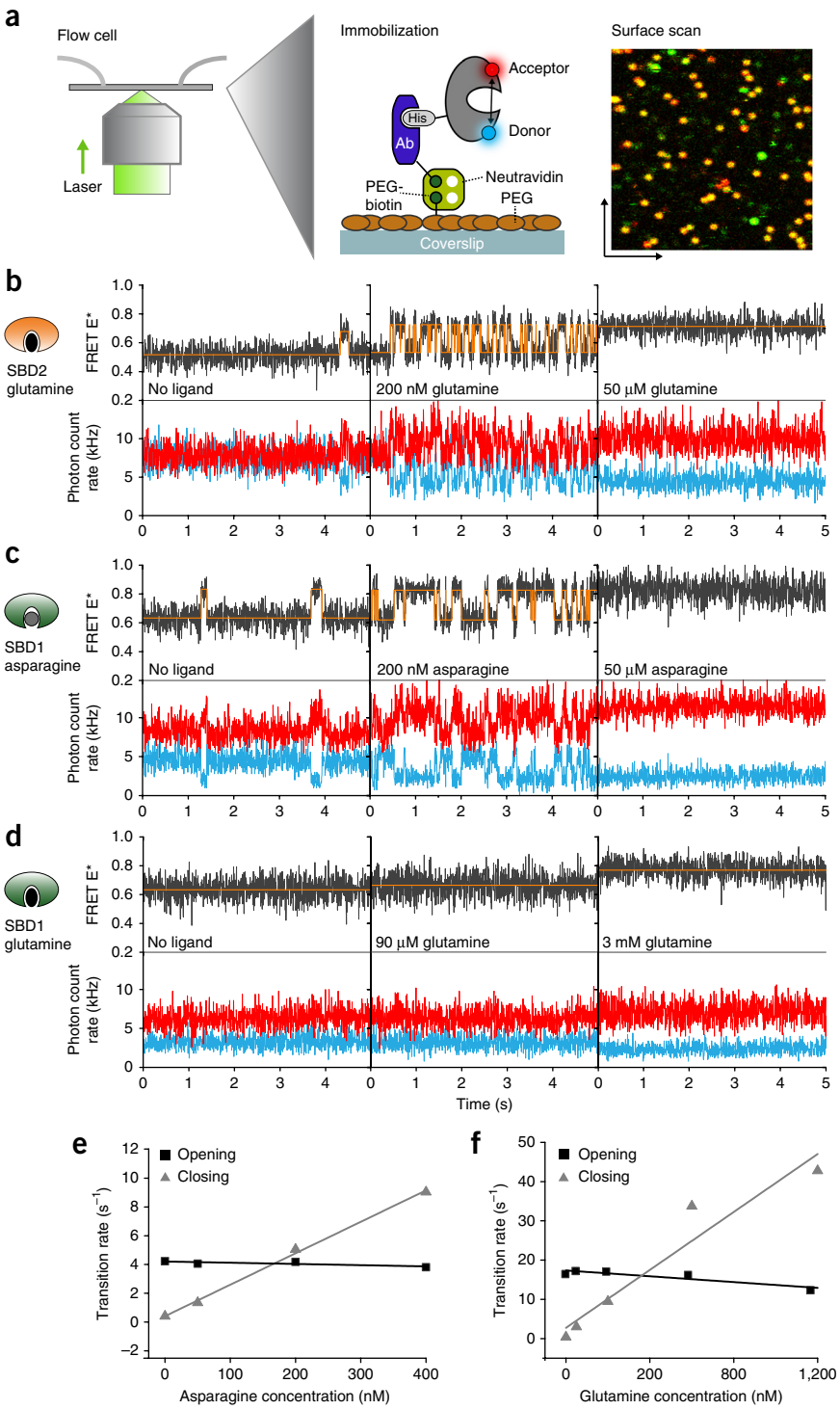

Figure 3 Single-molecule dynamics of surface-tethered SBDs probed by confocal scanning smFRET. (**a**) Schematic showing the immobilization of SBDs to the surface: histidine-tagged, dye-labeled SBDs were immobilized to a PEG-biotin–coated surface in a flow cell by biotinylated anti-His_5 antibody (Ab). A typical surface scan is shown in false-color representation at right (orange, double-labeled SBDs; green, SBDs with donor fluorophore only; red, SBDs with acceptor fluorophore only). (**b**–**d**) Representative fluorescence time traces (blue, donor signal; red, acceptor signal; gray, FRET signal; orange, fit) of SBDs labeled with Cy3B- and Atto647N-maleimide for SBD2 (T369C S451C) with the indicated concentrations of glutamine (**b**), SBD1(T159C G87C) with asparagine (**c**) and SBD1(T159C G87C) with glutamine (**d**). Statistics on time traces are presented in **Supplementary Table 2**. A detailed study on the intrinsic closing behavior in the presence of glutamine is provided in **Supplementary Figure 4a**,**b**. (**e**,**f**) Opening ($k_{opening}$) and closing ($k_{closing}$) rate constants of SBD1 (**e**) and SBD2 (**f**), determined from the transition rates of surface-immobilized molecules as a function of substrate concentration. The $k_{closing}$ was obtained from the slope of the linear fit and is indicative of first-order kinetics. The $k_{opening}$ follows zero-order kinetics.

to a state with FRET efficiencies of ~0.70 for SBD2 and ~0.83 for SBD1, which are identical to values for the closed conformation observed with the high-affinity ligands. SBD2 and SBD1 transited intrinsically to their closed conformation C (**Fig. 2a**) on average every 2.5 s (**Supplementary Table 2**). The average dwell times of the closed ligand-free state (τ_{closed}) are ~60 ms for SBD2 and ~240 ms for SBD1 (**Supplementary Table 2**).

SBD1 and SBD2 bind ligands via an induced-fit mechanism

Next, we analyzed the kinetics of opening and closing of the SBDs as a function of substrate concentration. The opening rates were concentration independent, whereas the closing of SBD1 and SBD2 increased with substrate concentration (**Fig. 3b**–**f** and **Table 1**). Remarkably, the lifetimes of the closed state were similar in the absence and presence of high-affinity ligand for both SBD2 (glutamine) and SBD1 (asparagine), thus indicating that the ligand does not 'stabilize' the closed conformation relative to the transition state. In contrast, we found that the transitions between open and closed states were extremely fast (<1 ms) when the low-affinity ligand glutamine binds to SBD1 (**Fig. 3d**). These fast transitions are distinct from the intrinsic slow transitions (**Fig. 3b**,**c** and **Supplementary Fig. 4**). This implies that glutamine shortens the lifetime of the closed state. With our current time resolution, we cannot rule out that SBD1 shows either fast submillisecond dynamics between O and CL or a structurally distinct partially closed state when the low-affinity ligand is bound. The smFRET data are in accordance with thermal unfolding experiments (data not shown), which reveal a lower degree of stabilization by saturating amounts of glutamine than asparagine.

We conclude from the smFRET measurements on surfaces that (i) SBD1 and SBD2 display intrinsic dynamics to the closed conformation; (ii) the binding of high-affinity ligands enhances transition of SBD1 and SBD2 to the closed state more frequently but without relative stabilization of this conformation; (iii) binding of glutamine to SBD1 shortens the closed-state lifetime; and (iv) in all cases, the binding reaction follows first-order kinetics, whereas the release reaction

Table 1 Rate constants for closing and opening of SBDs

		$k_{closing}$ (s^{-1} M^{-1})	$k_{opening}$ (s^{-1})
SBD2(T369C S451C)	Glutamine	3.8×10^7	17.2
SBD1(T159C G87C)	Asparagine	2.2×10^7	4.2
SBD1(T159C G87C E184D V185E)	Asparagine	7.3×10^6	10.8
SBD1(T159C G87C E184D V185E)	Glutamine	7.1×10^6	3.6
SBD2(T369C S451C D417F)	Glutamine	NA	NA

The table summarizes the results of smFRET with surface-bound proteins for the SBDs analyzed in this study (data presented in **Figs. 3–5** and **Supplementary Figs. 4** and **6**). NA, not applicable.

is of zeroth order (independent of ligand concentration). Collectively, these data are compatible with the induced-fit mechanism (**Fig. 2a**), despite the unique feature of intrinsic closing of the binding sites. This could well represent a generic feature of substrate-binding proteins associated with type I ABC transporters because similar observations have been made for mutants of maltose-binding protein[33].

The closed state of SBD2 interacts with the TMD

It is still debated how and which states of SBDs dock on the translocator complex[16,17,26]. GlnPQ is an excellent model system to address these questions because (i) it has multiple SBDs that compete with each other for interaction with the TMDs; (ii) the covalent linkage of the SBDs to the TMD ensures a high and fixed concentration of receptor protein available for transport; and (iii) the selectivity of the SBDs is different, thus allowing the paths of transport from SBD1 and SBD2 and their mutual influence to be dissected. Because both SBD1 and SBD2 show intrinsic closing without involvement of the ligand, we can directly probe whether the closed ligand-free state of, for example, SBD2 competes with SBD1-facilitated transport of asparagine, the amino acid that is not bound by SBD2.

We designed a mutation on SBD2 that abolishes glutamine binding (binding site of SBD2 and the position of the D417F substitution shown in **Fig. 4a**). Indeed, D417F abolished glutamine binding (**Supplementary Fig. 1c**), and GlnPQ-SBD2(D417F) no longer transported glutamine (**Supplementary Fig. 1c**). We set out to find the conformations of the 'trapped' state of SBD2(D417F). SBD2(D417F) had a melting temperature (in thermal unfolding experiments) and an elution profile (in size-exclusion chromatography) similar to those of SBD2, thus indicating that the apoprotein folds normally (data not shown). smFRET measurements in solution showed that the protein has a similar open conformation in the absence of ligand as that of SBD2 (**Supplementary Fig. 5a**). SBD2(D417F) did not undergo detectable conformational changes upon addition of 20 mM glutamine (**Supplementary Fig. 5b**). With surface-immobilized protein, we found that SBD2(D417F) is solely in the open conformation and lacks the capacity to transit intrinsically to the closed state (**Fig. 4b** and **Table 1**). Over periods of 30–60 s we did not find a single closing event, thus indicating that the protein is trapped in the open ligand-free state.

Next, we investigated the impact of the D417F mutation in the context of the full-length transporter (**Fig. 4c**). We found that GlnPQ(D417F) has about 50% of the glutamine-uptake activity of GlnPQ (**Fig. 4d**). Strikingly, the rate of asparagine uptake by GlnPQ(D417F) was almost three-fold higher than that of GlnPQ, although both proteins were expressed at similar levels (**Fig. 4d**). This suggests that the open ligand-free conformation of SBD2(D417F) no longer (or poorly) interacts with the TMDs. It implies that in GlnPQ, SBD2 competes with SBD1 for delivery of the substrate to the TMD, even in the absence of the SBD2 substrate. In fact, given the fraction of time in which the ligand-free and ligand-bound SBD2 are in the closed state, the closed ligand-free conformation of SBD2 inhibits transport at least an order of magnitude more strongly than the closed ligand-bound structure does (**Fig. 4e**). At first glance, this finding is counterintuitive because SBD2 visits the closed state only once every 2.5 s. However, SBD2's $k_{closing}$ of 0.4 s^{-1} is within the range of the duration of a full translocation cycle of GlnPQ. Taking the GlnPQ expression at 1–2% of total membrane protein, the observed transport rate of 5 nmol min^{-1} mg^{-1} corresponds to a turnover number of 0.25–0.5 s^{-1}. Thus, the intrinsic closing of SBD2 could well be a determining factor for the transport of asparagine via SBD1. Our transport experiments (**Fig. 4e**) show that the C state of SBD2 competes more severely with SBD1 than does CL; this is indicative of a blocked intermediate state. Under physiological conditions (i.e., with glutamine present), the CL state of SBD2 will be more prominent than C.

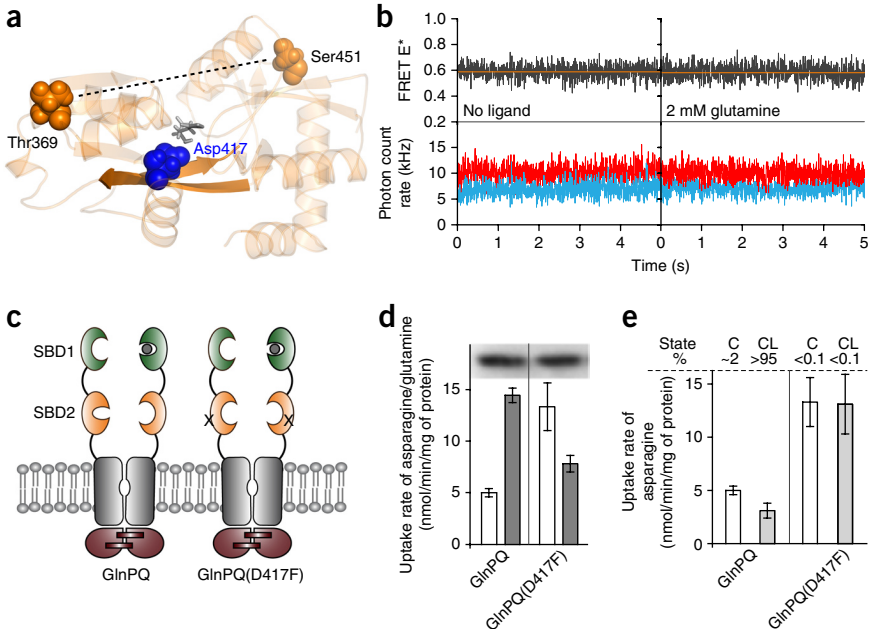

Figure 4 The closed ligand-free state of SBD2 inhibits transport via SBD1. (**a**) Crystal structure of the closed state of SBD2 showing the positions (T369C and S451C, orange spheres) used for fluorophore labeling (as in **Fig. 2b**). Asp417 (blue spheres); glutamine (gray sticks) and the hinge region (two nontransparent β-sheets) are depicted. (**b**) smFRET analysis of SBD2(D417F) labeled at Cys369 and Cys451 with Cy3B- and Atto647N-maleimide. (**c**) Schematic of GlnPQ and GlnPQ(D417F). (**d**) Transport assays with 250 μM [^{3}H]asparagine (open bars) and [^{14}C]glutamine (filled bars) in *L. lactis* GKW9000 complemented with either GlnPQ or GlnPQ(D417F). Error bars, s.e.m. calculated from independent cell cultures ($n = 3$). Uncropped image of gel is shown in **Supplementary Data Set 1**. (**e**) Uptake of [^{3}H]asparagine by GlnPQ or GlnPQ(D417F) as in **d**, in the absence (open bars) or presence (filled bars) of 250 μM glutamine. The percentage of time SBD2 spends in the CL or C states is indicated (calculated from the smFRET data, **Supplementary Table 2**).

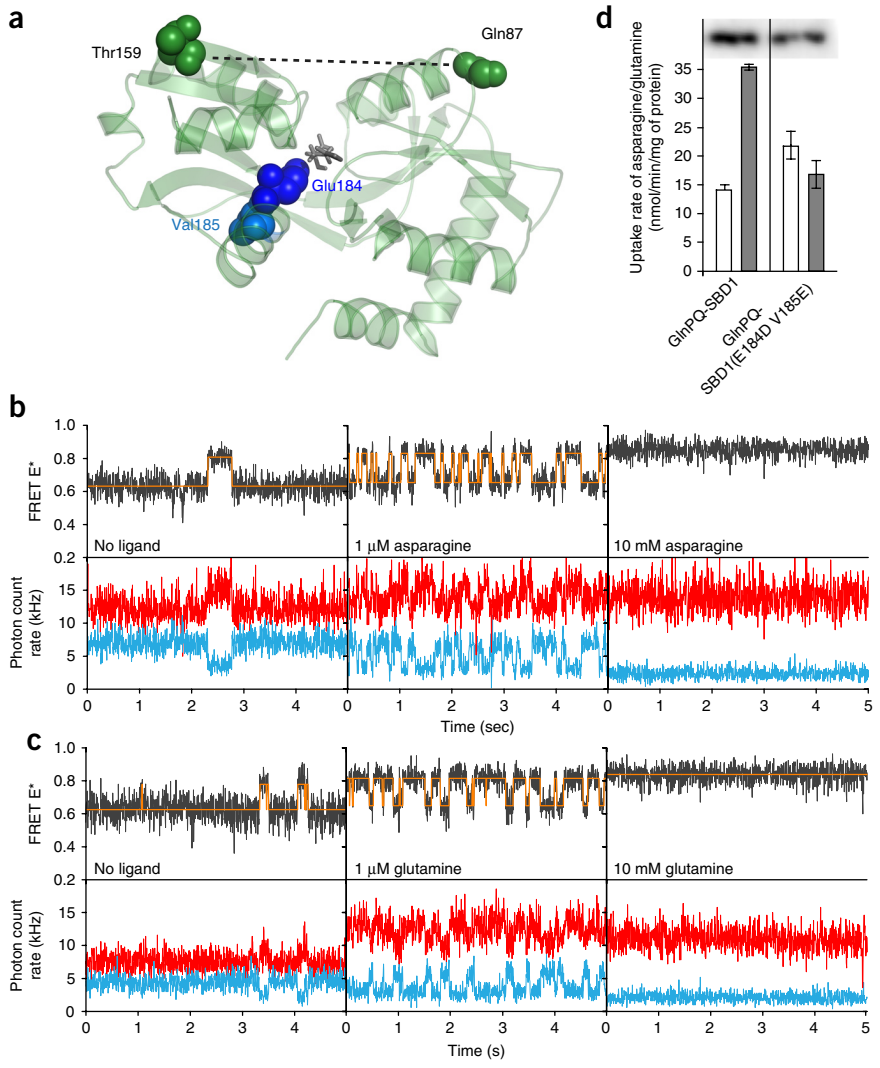

Figure 5 The closed-state lifetime of SBD1 influences the rate of transport. (**a**) The closed state of SBD1, modeled from the closed ligand-bound state of SBD2 with bound glutamine (PDB 4KQP[11]) as a template, with the SWISS-MODEL server (http://swissmodel.expasy.org/)[35–38]. T159C and G87C are indicated (green spheres). The E184D and V185E mutations (dark and light blue spheres, respectively) make the binding site of SBD1 similar to that of SBD2. Glutamine is shown in gray sticks. (**b**,**c**) smFRET traces of SBD1(E184D V185E) labeled at T159C and G87C with Cy3B- and Atto647N-maleimide. Representative fluorescence time traces are shown (blue, donor signal; red, acceptor signal; gray, FRET signal; orange, fit) in the absence or presence of ligand, as in **Figure 3b**,**c**. Statistics on time traces are presented in **Supplementary Table 2**. (**d**) Transport assays with 250 µM [^{3}H]asparagine (open bars) and [^{14}C]glutamine (filled bars) in *L. lactis* GKW9000 complemented with either GlnPQ-SBD1 or GlnPQ-SBD1(E184D V185E). Error bars, s.e.m. calculated from independent cell cultures ($n = 3$). The relative amount of GlnPQ-SBD1 and GlnPQ-SBD1(E184D V185E) was determined by immunoblotting as described in **Figure 1d**. Uncropped image of gel is shown in **Supplementary Data Set 1**.

The impact of induced fit and intrinsic closing on transport

The insights on substrate binding and release have been used to dissect the mechanistic role of SBD1 and SBD2 in transport. A different contact mode with the TMDs could explain the approximately two-fold difference in V_{max} when glutamine transport is compared in GlnPQ-SBD1 and GlnPQ-SBD2 (**Supplementary Fig. 1c**). Alternatively (or additionally), differences in substrate affinity and dwell times of the CL state may influence transport. Guided by the crystal structures[11], we designed E184D and V185E mutations (**Fig. 5a**). These substitutions resulted in a 100-fold increase in affinity for glutamine and an almost ten-fold decrease in affinity for asparagine (**Supplementary Fig. 1c**). ALEX measurements showed that asparagine and glutamine switch SBD1(E184D V185E) from the open to the closed state in the low-micromolar range, in agreement with the ITC measurements (**Supplementary Fig. 6a**,**b**). For both ligands, we observed two clearly resolved populations around their respective K_d values (**Supplementary Fig. 6a**,**b**). smFRET of SBD1(E184D V185E) immobilized on a surface showed that, relative to the lifetime of SBD1, the lifetime of the closed ligand-free state was lowered from ~240 to ~150 ms (**Supplementary Table 2**). The τ_{closed}(asparagine) was reduced from ~250 ms in SBD1 to ~110 ms in SBD1(E184D V185E). Consistently with the large increase in affinity, τ_{closed}(glutamine) increased from <1 ms to 280 ms (**Fig. 5b**,**c** and **Supplementary Tables 1** and **2**).

Next, we evaluated the impact of the E184D V185E double mutation on the transport of asparagine and glutamine. For GlnPQ-SBD1, we found, under saturating conditions, rates of asparagine and glutamine transport of ~21 and 38 nmol min^{-1} mg^{-1} protein, respectively (**Fig. 5d**). Remarkably, for GlnPQ-SBD1(E184D V185E), the activities were reversed, with V_{max}(asparagine) ≈ 27 and V_{max}(glutamine) ≈ 17 nmol min^{-1} mg^{-1} protein, respectively (**Fig. 5d**). Thus, by increasing the dwell time (τ_{closed}) of SBD1 for glutamine from <1 ms (wild type) to ~280 ms (E184D V185E), the rate of glutamine uptake decreased two-fold. Consistently with this, the decrease of τ_{closed}(asparagine) from ~250 to ~110 ms parallels an increase in the asparagine transport rate. These findings confirm that the delivery of the substrate is an important step influencing the overall translocation.

DISCUSSION

Using the collective data on ligand binding and transport, we have constructed a scheme of the translocation cycle of GlnPQ also taking into account published data on the maltose ABC importer[34]. Substrates are captured via SBDs (**Fig. 6**, S_I), which then undergo a conformational change to a closed state, according to the induced-fit mechanism (**Fig. 6**, S_{II}). Occasionally, the SBDs of GlnPQ intrinsically close, and the translocation cycle is inhibited when the C conformation binds to the TMD (**Fig. 6**, S_{III}*). Instead, SBDs in the CL conformation lead to the pre-translocation state (**Fig. 6**, S_{III}) upon docking onto an inward-facing TMD. ATP induces NBD dimerization, and an outward-facing TMD is formed for substrate transfer (**Fig. 6**, S_{IV}). Subsequently, ATP hydrolysis and release of P_i and ADP complete the translocation (**Fig. 6**, S_V); upon binding of ATP (**Fig. 6**, S_I) the transporter is ready for a new cycle.

We performed kinetic modeling based on differential equations to describe the dynamics of the GlnPQ translocation cycle and to

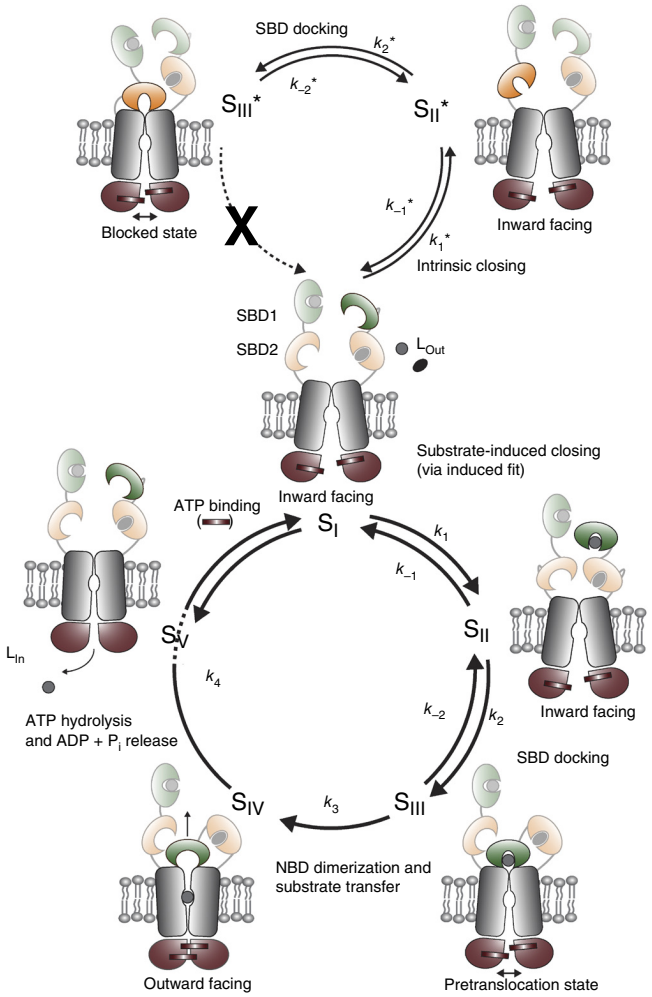

Figure 6 Model of the translocation cycle of GlnPQ. The model is based on the work presented here for GlnPQ and builds on previous studies of the type I ABC transporter for maltose[34]. SBD1 and SBD2 are indicated in green and orange, respectively, and asparagine and glutamine are depicted as gray circles and black ovals, respectively. TMDs and NBDs are labeled in gray and brown, respectively. Substrate binding via an induced-fit mechanism induces a conformational change of the SBDs from O (S_I) to CL (S_{II}) that interacts with the resting state of the transporter, thus leading to the pretranslocation state (S_{III}). Subsequently, opening of the SBD upon ATP-induced dimerization of the NBDs drives the transporter to the outward-facing conformation (S_{IV}), and the substrate is transferred through the TMDs (S_V). ATP hydrolysis and release of P_i and ADP resets the transporter to the initial resting state (S_I) for a new transport cycle. The C state of the SBD can also interact with the transporter, and it (reversibly) inhibits the translocation ($S_{II}^* \rightarrow S_{III}^*$). A rate constant k is assigned to each step as indicated and is used in the kinetic model as described in **Supplementary Note 1**.

find out whether the model is consistent with our experimental data (**Supplementary Note 1**). The K_m/K_d ratio can be >1 (SBD1-Asn), ~1 (SBD2-Gln) or <1 (SBD1-Gln) (**Supplementary Fig. 1c**); this indicates that, depending on the SBD or substrate, different steps in the translocation cycle are rate determining. Furthermore, the lifetime of the closed state varies with the SBD and substrate, and C or CL inhibit transport differently. In the model, the translocation cycle is represented by seven steps whose kinetics depend on the SBD, the substrate or both. To compute the transport rate, we put the system in steady state.

The model predicts the following: (i) The lifetime of CL influences the transition to the outward-facing conformation ($S_{III} \rightarrow S_{IV}$). Long-lived closed conformations impede the transition and thus the transfer of the substrate, rendering the overall transport inefficient. (ii) The lifetime of the closed conformation is shortened relative to that of free SBD when the SBD–translocator complex transits through step S_{III} to S_{IV}. Thus, ATP-induced NBD dimerization and associated conformational rearrangements in the TMD facilitate SBD opening. (iii) Docking ($S_{II} \rightarrow S_{III}$) is more efficient for SBD2 than SBD1, thus favoring the transport of the essential amino acid glutamine over that of asparagine. (iv) The final step in translocation ($S_{IV} \rightarrow S_V$) is more efficient with asparagine than glutamine, hence the high K_m/K_d ratio for asparagine (equation (8) in **Supplementary Note 1**). This also implies that the substrate, transferred to the TMD, acts as a trigger for subsequent steps, for example, the stimulation of ATP hydrolysis and/or P_i and ADP release, and is consistent with the stronger inhibition of transport by C than by CL.

The maximal rate of substrate uptake, V_{max}, is inversely proportional to the total time of docking ($S_{II} \rightarrow S_{III}$), opening and release of ligand from the docked SBD ($S_{III} \rightarrow S_{IV}$) and the final step in translocation ($S_{IV} \rightarrow S_V$) (equation (7) in **Supplementary Note 1**). Although transport via SBD1 and SBD2 cannot be compared directly (because the critical interactions with the TMD may differ), the much shorter lifetime of the closed state of SBD2 ($\tau_{closed} \approx 60$ ms) than that of SBD1 ($\tau_{closed} \approx 250$ ms) is consistent with a much faster transport rate. Taken together, and in agreement with the model, the differences in V_{max} and K_m/K_d indicate that, depending on the SBD or substrate, different steps in the translocation cycle are rate determining. For asparagine import via SBD1, the substrate delivery ($S_I \rightarrow S_{II}$ and $S_{II} \rightarrow S_{III}$) is more rate determining, and for glutamine import via SBD2 the final translocation step is more rate determining ($S_{IV} \rightarrow S_V$).

Our kinetic model is consistent with published data on type I ABC transporters, but it also makes new predictions such as the importance of the lifetime of the closed ligand-bound state and the role of the substrate (rather than SBD) in triggering later steps of the translocation cycle. The results on the E184D V185E mutant are important for the validation of the model. We find that glutamine is transported two-fold faster than asparagine when SBD1 is used. In SBD1(E184D V185E) the specificity is reversed, and asparagine is transported faster than glutamine. In fact, the rates of transport correlate with the lifetime of CL. Intrinsically this lifetime is long (for example, ~240 ms for SBD1) and not affected by the binding of high-affinity ligand. In the E184D V185E mutant, we lower the lifetime of CL for asparagine and increase the lifetime for glutamine, and the transport rates change reciprocally; this is consistent with a long-lived state limiting translocation.

In summary, we find that high-affinity binding proceeds via the induced-fit mechanism, and the lifetime of the closed state of the substrate-binding domain is a determining factor for the rate of transport. The opening of the substrate-binding domains seems to be linked to the transition of TMD from inward to outward facing. Moreover, we find that SBDs compete with each other in the closed state, but the extent of inhibition is stronger without ligand. Our findings contribute to a general understanding of the mechanism of ABC transport, information obtained for the first time, to our knowledge, by single-molecule structural studies and a kinetic analysis of substrate translocation.

METHODS

Methods and any associated references are available in the online version of the paper.

Note: Any Supplementary Information and Source Data files are available in the online version of the paper.

ACKNOWLEDGMENTS

We thank S. Weiss (University of California Los Angeles) and A.N. Kapanidis (University of Oxford) for providing software for data acquisition and analysis of ALEX data. This work was supported by grants from the Netherlands Organization for Scientific research (NWO; Top-subsidy grant 700.56.302 to B.P.), the Marie-Curie Initial Training Networks program Network for Integrated Cellular Homeostasis (NICHE) (coordinated by B.P.) and the Zernike Institute for Advanced Materials and the Centre for Synthetic Biology (University of Groningen startup grant to T.C.). G.G. is supported by a NWO-VENI grant (grant no. 722.012.012). E.P. acknowledges a postdoctoral fellowship from the German Science Foundation (DFG; grant PL696/2-1). We thank R.M. Scheek for assistance with the data analysis.

AUTHOR CONTRIBUTIONS

G.G., G.K.S.-W., E.P., M.d.B., T.C. and B.P. designed experiments and analyzed and interpreted the data. G.G., G.K.S.-W., E.P., F.H., R.V. and T.C. performed experiments. G.G., G.K.S.-W., E.P., T.C. and B.P. wrote the manuscript. All authors approved the final version of the manuscript.

COMPETING FINANCIAL INTERESTS

The authors declare no competing financial interests.

1. Higgins, C.F. ABC transporters: from microorganisms to man. *Annu. Rev. Cell Biol.* **8**, 67–113 (1992).
2. Biemans-Oldehinkel, E., Doeven, M.K. & Poolman, B. ABC transporter architecture and regulatory roles of accessory domains. *FEBS Lett.* **580**, 1023–1035 (2006).
3. Biemans-Oldehinkel, E., Mahmood, N.A. & Poolman, B. A sensor for intracellular ionic strength. *Proc. Natl. Acad. Sci. USA* **103**, 10624–10629 (2006).
4. Rees, D.C., Johnson, E. & Lewinson, O. ABC transporters: the power to change. *Nat. Rev. Mol. Cell Biol.* **10**, 218–227 (2009).
5. Doeven, M.K., Abele, R., Tampe, R. & Poolman, B. The binding specificity of OppA determines the selectivity of the oligopeptide ATP-binding cassette transporter. *J. Biol. Chem.* **279**, 32301–32307 (2004).
6. van der Heide, T. & Poolman, B. Osmoregulated ABC-transport system of *Lactococcus lactis* senses water stress via changes in the physical state of the membrane. *Proc. Natl. Acad. Sci. USA* **97**, 7102–7106 (2000).
7. Sharom, F.J. ABC multidrug transporters: structure, function and role in chemoresistance. *Pharmacogenomics* **9**, 105–127 (2008).
8. Nagao, K., Kimura, Y., Mastuo, M. & Ueda, K. Lipid outward translocation by ABC proteins. *FEBS Lett.* **584**, 2717–2723 (2010).
9. Holland, I.B., Cole, S.P., Kuchler, K. & Higgins, C.F. *ABC Proteins: from Bacteria to Man* (Academic Press, 2003).
10. van der Heide, T. & Poolman, B. ABC transporters: one, two or four extracytoplasmic substrate-binding sites? *EMBO Rep.* **3**, 938–943 (2002).
11. Fulyani, F. *et al.* Functional diversity of tandem substrate-binding domains in ABC transporters from pathogenic bacteria. *Structure* **21**, 1879–1888 (2013).
12. Davidson, A.L., Dassa, E., Orelle, C. & Chen, J. Structure, function, and evolution of bacterial ATP-binding cassette systems. *Microbiol. Mol. Biol. Rev.* **72**, 317–364 (2008).
13. Oldham, M.L., Davidson, A.L. & Chen, J. Structural insights into ABC transporter mechanism. *Curr. Opin. Struct. Biol.* **18**, 726–733 (2008).
14. Locher, K.P. Structure and mechanism of ATP-binding cassette transporters. *Phil. Trans. R. Soc. Lond. B* **364**, 239–245 (2009).
15. Oldham, M.L., Khare, D., Quiocho, F.A., Davidson, A.L. & Chen, J. Crystal structure of a catalytic intermediate of the maltose transporter. *Nature* **450**, 515–521 (2007).
16. Khare, D., Oldham, M.L., Orelle, C., Davidson, A.L. & Chen, J. Alternating access in maltose transporter mediated by rigid-body rotations. *Mol. Cell* **33**, 528–536 (2009).
17. Bao, H. & Duong, F. ATP alone triggers the outward facing conformation of the maltose ATP-binding cassette transporter. *J. Biol. Chem.* **288**, 3439–3448 (2013).
18. Schuurman-Wolters, G.K. & Poolman, B. Substrate specificity and ionic regulation of GlnPQ from *Lactococcus lactis*: an ATP-binding cassette transporter with four extracytoplasmic substrate-binding domains. *J. Biol. Chem.* **280**, 23785–23790 (2005).
19. Berntsson, R.P.A., Smits, S.H.J., Schmitt, L., Slotboom, D.-J. & Poolman, B. A structural classification of substrate-binding proteins. *FEBS Lett.* **584**, 2606–2617 (2010).
20. Clore, G.M. Interplay between conformational selection and induced fit in multidomain protein-ligand binding probed by paramagnetic relaxation enhancement. *Biophys. Chem.* **186**, 3–12 (2014).
21. Tang, C., Schwieters, C.D. & Clore, G.M. Open-to-closed transition in apo maltose-binding protein observed by paramagnetic NMR. *Nature* **449**, 1078–1082 (2007).
22. Csermely, P., Palotai, R. & Nussinov, R. Induced fit, conformational selection and independent dynamic segments: an extended view of binding events. *Trends Biochem. Sci.* **35**, 539–546 (2010).
23. Kim, E. *et al.* A single-molecule dissection of ligand binding to a protein with intrinsic dynamics. *Nat. Chem. Biol.* **9**, 313–318 (2013).
24. Oldham, M.L. & Chen, J. Crystal structure of the maltose transporter in a pretranslocation intermediate state. *Science* **332**, 1202–1205 (2011).
25. Oldham, M.L., Khare, D., Quiocho, F.A., Davidson, A.L. & Chen, J. Crystal structure of a catalytic intermediate of the maltose transporter. *Nature* **450**, 515–521 (2007).
26. Oldham, M.L. & Chen, J. Crystal structure of the maltose transporter in a pretranslocation intermediate state. *Science* **332**, 1202–1205 (2011).
27. Mao, B., Pear, M.R., Mccammon, J.A. & Quiocho, F.A. Hinge-bending in L-arabinose-binding protein: the venus-flytrap model. *J. Biol. Chem.* **257**, 1131–1133 (1982).
28. Bermejo, G.A., Strub, M.P., Ho, C. & Tjandra, N. Ligand-free open-closed transitions of periplasmic binding proteins: the case of glutamine-binding protein. *Biochemistry* **49**, 1893–1902 (2010).
29. Ha, T. *et al.* Probing the interaction between two single molecules: fluorescence resonance energy transfer between a single donor and a single acceptor. *Proc. Natl. Acad. Sci. USA* **93**, 6264–6268 (1996).
30. Kapanidis, A.N. *et al.* Fluorescence-aided molecule sorting: analysis of structure and interactions by alternating-laser excitation of single molecules. *Proc. Natl. Acad. Sci. USA* **101**, 8936–8941 (2004).
31. Lee, N.K. *et al.* Accurate FRET measurements within single diffusing biomolecules using alternating-laser excitation. *Biophys. J.* **88**, 2939–2953 (2005).
32. van der Velde, J.H.M. *et al.* Mechanism of intramolecular photostabilization in self-healing cyanine fluorophores. *ChemPhysChem* **14**, 4084–4093 (2013).
33. Seo, M.-H., Park, J., Kim, E., Hohng, S. & Kim, H.-S. Protein conformational dynamics dictate the binding affinity for a ligand. *Nat. Commun.* **5**, 3724 (2014).
34. Chen, J. Molecular mechanism of the *Escherichia coli* maltose transporter. *Curr. Opin. Struct. Biol.* **23**, 492–498 (2013).
35. Arnold, K., Bordoli, L., Kopp, J. & Schwede, T. The SWISS-MODEL workspace: a web-based environment for protein structure homology modelling. *Bioinformatics* **22**, 195–201 (2006).
36. Biasini, M. *et al.* SWISS-MODEL: modelling protein tertiary and quaternary structure using evolutionary information. *Nucleic Acids Res.* **42**, W252–W258 (2014).
37. Guex, N., Peitsch, M.C. & Schwede, T. Automated comparative protein structure modeling with SWISS-MODEL and Swiss-PdbViewer: a historical perspective. *Electrophoresis* **30** (suppl. 1), S162–S173 (2009).
38. Kiefer, F., Arnold, K., Kunzli, M., Bordoli, L. & Schwede, T. The SWISS-MODEL Repository and associated resources. *Nucleic Acids Res.* **37**, D387–D392 (2009).

ONLINE METHODS

Nomenclature of GlnPQ derivatives. GlnPQ is composed of two GlnP and two GlnQ subunits. GlnP corresponds to the transmembrane domain (TMD) to which the substrate-binding domains SBD1 and SBD2 are linked N terminally[18]. GlnP is synthesized as a preprotein, and the Sec-dependent N-terminal signal sequence (preceding SBD1) is cleaved off after the translocation of the SBDs across the membrane[39]. GlnQ corresponds to the nucleotide-binding domain (NBD). The wild-type transporter is referred to as GlnPQ, and the systems lacking SBD1 or SBD2 or both are referred to as GlnPQ-SBD2, GlnPQ-SBD1 and GlnPQ-ΔSBD, respectively. Site-directed mutations to alter the binding properties of the full-length transporter or one of the SBDs are named as, for example, GlnPQ(D417F) and SBD2(D417F), in which the number refers to the position predicted from the full-length gene. In discussing the properties of individual mutants, for example, SBD2(D417F), the mutations to create the cysteine residues for labeling with fluorophores are not indicated. We have made several cysteine pairs and used only those that showed wild-type activity after modification, and for convenience these mutations are not indicated in the main text but are specified in the figure legends. The SBD1 derivatives used in smFRET studies are based on SBD1(G87C T159C) unless otherwise indicated, and the SBD2 derivatives are based on SBD2(T369C S451C) (**Supplementary Fig. 2a**).

Bacterial strains, growth conditions and membrane vesicle preparation. *L. lactis* strains (NZ9000 and GKW9000) were cultivated semianaerobically at 30 °C in M17 medium supplemented with 1% (w/v) glucose and 5 μg/ml chloramphenicol when carrying pNZglnPQhis or other derivatives. The soluble substrate-binding domains were expressed in *E. coli* strain MC1061 carrying pBADnLicSBD1 and pBADnLicSBD2 and derivatives (site-directed mutants in either SBD1 or SBD2). The cells were grown in Luria-Bertani medium supplemented with 100 μg/ml of ampicillin in shake flasks. Expression was triggered at an OD_{600} of 0.5–0.6 by addition of 2×10^{-4}% L-arabinose, and fermentation was continued for another 2 h. Cells were harvested by centrifugation (15 min, 6,000*g*) and washed once with 100 mM KP_i (pH 7.5). After resuspension in 50 mM KP_i (pH 7.5), 20% glycerol with 0.1 mg/ml DNase and 1 mM PMSF, the cells were disrupted by sonication. The supernatant (after disruption of the cells) was collected after ultracentrifugation (90 min, 150,000*g*) and stored at −80 °C after being flash frozen in liquid nitrogen.

Cloning and mutagenesis. M17 broth was obtained from Oxoid, and Gistex LS from Brenntag. Radiolabeled L-[^{3}H]asparagine (20 Ci/mmol) was obtained from ARC Radiochemicals, and L-[^{14}C]glutamine (50 mCi/mmol) was obtained from PerkinElmer. All other chemicals were of analytical grade and were obtained from commercial sources. A *glnPQ*-deletion mutant was constructed in *L. lactis* NZ9000 by homologous recombination[40]. The replacement vector pORI280*glnPQ* lacks the *repA* gene, which is essential for replication and contains an erythromycin-resistance marker for positive selection and the β-galactosidase (*lacZ*) gene for blue-white screening. After transformation of NZ9000, which also lacks *repA*, with pORI280Δ*glnPQ*, the selection for growth was performed in the presence of erythromycin, thus isolating cells with integration of the plasmid into the chromosome. Erythromycin-resistant blue colonies were picked and grown under nonselective conditions in GM17 medium lacking erythromycin, thus selecting for a second recombination event. Subsequently, the screening was done on white colonies, which are erythromycin sensitive. This resulted in selection for either the looping out of the original plasmid pORI280*glnPQ* or the looping out of wild-type *glnPQ*. The knockout strain was named GKW9000, and the phenotype was confirmed by PCR on genomic DNA and by uptake experiments on whole cells.

The 3′ fragment of pORI280*glnPQ* starts 199 bp 5′ of the stop codon of *glnQ* and ends 655 bp 3′ of the stop codon, corresponding to a fragment of 854 bp flanked with an upstream *Sty*I, and downstream BglII site for cloning in pORI280. The 5′ fragment starts 1,019 bp 5′ of the initiation codon and ends 90 bp 3′ of the initiation codon of the *glnP* gene; at the end, an in-frame TAA stop codon was added before the *Sty*I restriction site. The resulting 1,109-bp fragment was cloned in pORI280, already containing the 3′ fragment, with EcoRI and *Sty*I.

The genes encoding the soluble SBDs were cloned into pBADnLIC[41], using ligation-independent cloning (LIC), thus resulting in an N-terminal extension of the proteins with a His_{10} tag and a TEV protease site as described. Site-directed mutagenesis was accomplished with the QuikChange Site-Directed Mutagenesis protocol (Stratagene), and mutations were verified by sequence analysis (Seqlab). Briefly, 100 ng of template DNA (pBADnLIC containing either the SBD1 or SBD2 gene described above) was mixed with 0.3 μM of forward and reverse mutagenic primers in a PCR reaction with PfuUltra High-Fidelity DNA polymerase (Stratagene). A control PCR reaction, in which addition of the polymerase was omitted, was also included. The PCR reaction mixture was treated with *Dpn*I (37 °C, 5 h) to digest the parental DNA, and this was followed by transformation into *E. coli* DH5α competent cells. The efficiency of the procedure was >90% (verified after sequencing), and the number of colonies varied from 50 to100, whereas in the control PCR reaction, no colonies were observed.

Purification of SBD1 and SBD2. The cell lysate was thawed and mixed with 50 mM KP_i, pH 8.0, 200 mM KCl and 20% glycerol (buffer A) plus 20 mM imidazole and incubated with Ni^{2+}-Sepharose resin (5.5-ml bed volume of Ni^{2+}-Sepharose per wet-weight gram of cells) for 1 h at 4 °C (under mild agitation). Next, the resin was washed with 20 column volumes of buffer A supplemented with 50 mM imidazole. The histidine-tagged proteins were eluted in three column volumes of buffer A supplemented with 500 mM imidazole. Immediately after elution and concentration determination, 5 mM EDTA was added to prevent aggregation of the proteins. The histidine tag was cleaved off by treatment with histidine-tagged TEV protease at a ratio of 1:40 (w/w) with respect to the purified protein, and subsequently the protein was dialyzed against 50 mM Tris-HCl, pH 8.0, 0.5 mM EDTA plus 0.5 mM DTT overnight at 4 °C. The histidine-tagged TEV protease and residual uncut protein was removed with a 0.5-ml bed volume of Ni^{2+}-Sepharose. The flow through of the column was concentrated (Vivaspin, Sartorius; ~5 mg/ml), dialyzed in buffer A supplemented with 50% glycerol, divided into aliquots and stored at −80 °C after flash freezing. Prior to experiments, all proteins were further purified with size-exclusion chromatography on a Superdex-200 column (GE Healthcare) equilibrated in 50 mM KP_i, pH 8.0, and 200 mM KCl. To make sure that no endogenous ligand was left, for some experiments, we unfolded the SBDs by treatment with 6 M of urea and refolded them again, as previously described[42]. The intrinsic dynamics of both SBD1 and SBD2 (**Fig. 3b**,**c** and **Supplementary Table 2**) were identical irrespective of the urea treatment, thus indicating that these are not related to endogenous ligand in the sample.

Calorimetric measurements. Isothermal titration calorimetry (ITC) experiments were performed as described previously[11]. Briefly, the purified SBDs were dialyzed overnight against 50 mM KP_i, pH 6.0, 1 mM EDTA and 1 mM NaN_3. Isothermal titration experiments were carried out with an ITC-200 (MicroCal, GE Healthcare). For these experiments, the substrate was prepared in the dialysis buffer to minimize mixing effects. All experiments were carried out at 25 °C with a mixing rate of 1,000 r.p.m.

Uptake experiments in whole cells. Cells were grown in GM17 to an OD_{600} of 0.4, induced for 1 h with 0.01% of culture supernatant of the nisin A–producing strain NZ9700 (containing 10 μg/L of nisin A) and harvested by centrifugation for 10 min at 4,000*g*. After being washed twice with 10 mM PIPES-KOH, 80 mM KCl, pH 6.0, the cells were resuspended to OD_{600} 50 in the same buffer. Uptake experiments were performed at final protein concentrations of 2.5–250 μg/ml in 30 mM PIPES-KOH, 30 mM MES-KOH, and 30 mM HEPES-KOH, pH 6.0. Before the transport assays, the cells were equilibrated and energized at 30 °C for 3 min in the presence of 10 mM glucose plus 5 mM $MgCl_2$. After 3 min, the uptake reaction was started by addition of either [^{14}C]glutamine or [^{3}H]asparagine; the specific radioactivity was adjusted in the different experiments to have disintegrations per minute (d.p.m.) at least ten-fold above the background. The final amino acid concentrations are indicated in the figures, tables and/or figure legends. At given time intervals, samples were taken and diluted in 2 ml ice-cold 100 mM LiCl. The samples were rapidly filtered through 0.45-μm cellulose nitrate filters (Whatman/GE Healthcare), and the filter was washed once with ice-cold 100 mM LiCl. The radioactivity on the filters was determined by liquid scintillation counting. Initial rates of transport were estimated from the linear part of uptake with time, as shown in **Supplementary Figure 1a**.

Quantification of the intracellular amount of GlnPQ derivatives. Leftover samples from the whole-cell uptake experiments were used to compare the expression levels between the different constructs. Typically, 150 μl of cell suspension of an

OD_{600} = 50 was diluted to 500 µl with washing buffer (10 mM PIPES-KOH and 80 mM KCl, pH 6.0), and 300 mg of 0.1-mm glass beads were added. Cells were ruptured for 5 min at 50 Hz with a tissue lyser (Qiagen). After the glass beads settled, the supernatant was used to load 48 µg of total protein onto a 12.5% SDS-PAGE gel. After separation, the gel was subjected to western blotting with a commercial anti-histidine antibody (5Prime, cat. no. 2400320 at 1:5,000 dilution; validation on manufacturer's website) for detecting GlnQ. The signal was visualized by chemiluminescence of alkaline phosphatase in a Fuji LAS-3000 imager.

Purification of cysteine-containing mutants and protein labeling. Unlabeled SBD1 and SBD2 cysteine-containing derivatives were stored at −20 °C in 100-µl aliquots of 20-40 mg/ml in 50 mM KP_i, pH 7.4, 50 mM KCl and 50% glycerol plus 1 mM DTT. Stochastic labeling with maleimide derivatives of donor and acceptor fluorophores was carried out on ~5 nmol of protein; SBD derivatives were labeled with Cy3B- and Atto747N-maleimide in a ratio of protein/Cy3B/Atto647N of 1:4:5. Briefly, purified proteins were treated with DTT (10 mM; 30 min) to fully reduce oxidized cysteines. After dilution of the protein sample to a DTT concentration of 1 mM the reduced protein was bound to a Ni^{2+}-Sepharose resin (GE Healthcare) and washed with ten column volumes of 50 mM KP_i, pH 7.4, 50 mM KCl and 10% glycerol (buffer B). Simultaneously, the applied fluorophore stocks (50 nmol in powder) dissolved in 5 µl of water-free DMSO, were added at appropriate amounts to buffer B and immediately applied to the protein bound to the Ni^{2+}-Sepharose resin (keeping the final DMSO concentration below 1%). The resin was incubated overnight and kept at 4 °C (under mild agitation). After labeling, unbound dye was removed by sequential washing with ten column volumes of buffer B, and this was followed by 100 column volumes of 50 mM KP_i, pH 7.4, 1 mM KCl and 50% glycerol. The protein was eluted in 0.8 ml of 50 mM KP_i, pH 7.4, 50 mM KCl, 5% glycerol and 500 mM imidazole, and was applied onto a Superdex-200 column (GE Healthcare) equilibrated with 50 mM KP_i, pH 7.4, and 200 mM KCl. We enriched for protein labeled with donor and acceptor fluorophores by taking advantage of the nonspecific interaction of the Atto647N dye with Superdex-200 column materials.

Additional methods. Further methodology can be found in **Supplementary Note 2**.

39. Blobel, G. & Dobberstein, B. Transfer of proteins across membranes. I. Presence of proteolytically processed and unprocessed nascent immunoglobulin light chains on membrane-bound ribosomes of murine myeloma. *J. Cell Biol.* **67**, 835–851 (1975).
40. Leenhouts, K. *et al.* A general system for generating unlabelled gene replacements in bacterial chromosomes. *Mol. Gen. Genet.* **253**, 217–224 (1996).
41. Geertsma, E.R. & Poolman, B. High-throughput cloning and expression in recalcitrant bacteria. *Nat. Methods* **4**, 705–707 (2007).
42. Lanfermeijer, F.C., Picon, A., Konings, W.N. & Poolman, B. Kinetics and consequences of binding of nona- and dodecapeptides to the oligopeptide binding protein (OppA) of *Lactococcus lactis*. *Biochemistry* **38**, 14440–14450 (1999).

doi:10.1038/nsmb.2929